Available online at www.sciencedirect.com

SCIENCE DIRECT®

International Journal of Solids and Structures 43 (2006) 899–912

INTERNATIONAL JOURNAL OF SOLIDS and STRUCTURES

www.elsevier.com/locate/ijsolstr

Finite element analysis of ink-tack delamination of paperboard

Nils Hallbäck [a,*], Orlando Girlanda [b,1], Johan Tryding [c]

[a] Karlstad University, Division for Engineering Sciences, Physics and Mathematics, SE-651 88 Karlstad, Sweden
[b] STFI-Packforsk, Drottning Kristinas väg 61, SE-114 86 Stockholm, Sweden
[c] Tetra Pak Carton Ambient AB, Ruben Rausings gata, SE-221 86 Lund, Sweden

Received 20 October 2004; received in revised form 8 June 2005
Available online 30 August 2005

Abstract

Finite element analysis of ink-tack delamination of paperboard were presented. The paperboard was modeled as a multilayered structure with a softening interface model connecting the paperboard plies. The paperboard plies were modeled as orthotropic linear elastic. The ink-tack loading was applied to the board in the form of a moving displacement boundary condition. The purpose of the analysis was to assess the influence from the elastic moduli of the individual layers on the ink-tack delamination event. The results indicated that in most cases of practical interest the board delaminated between the outer plies of the board, although the interface strength was lower in the middle of the board. This observation helped to explain why traditional tests for out-of-plane testing of paper by standardized methods could not uniquely predict the propensity for ink-tack delamination.

Keywords: Ink-tack delamination; Paperboard; Interface strength

1. Introduction

Delamination is an ubiquitous problem during offset printing operations on paperboard and coated paper grades. The delamination event is driven by the cohesive force that develops in the ink between the paper surface and the rubber blanket at the exit of the printing nip. This phenomenon is known as the ink-tack delamination phenomena (Franklin, 1980).

Ink is mainly composed of pigments, oils and binders. After application of the liquid ink to the substrate, the oil will be absorbed by the substrate with a resulting increase of the ink-tack of the remaining layer. The

* Corresponding author. Tel.: +46 54 700 21 15; fax: +46 54 700 14 49.
E-mail address: nils.hallback@kau.se (N. Hallbäck).
[1] Student at Karlstad University, Division for Engineering Sciences, Physics and Mathematics.

0020-7683/$ - see front matter
doi:10.1016/j.ijsolstr.2005.06.030

rate of oil absorption, or the setting speed of the ink, is a function of the substrate surface absorption. The ink-tack also increases with the velocity of the web, through the dynamic viscosity of the ink.

The substrate is released from the roll by ink-filamentation and rupture. Filamentation of the ink is caused by cavitation due to the pressure drop at the exit of the printing nip. The size and appearance of the filaments is a complex function of the fluid rheology and the printing speed (cf. Ercan and Bousfield, 2000; De Grâce et al., 1992). When the substrate sticks to the rubber blanket flexing of the web is achieved. The flexing of the web, in combination with the web tension, leads to an increased release angle which has been found to be central to the ink-tack delamination phenomenon (Franklin, 1980). The distance at which the substrate sticks to the rubber blanket depends on the ink-tack, the web tension and the flexibility of the web. Hence the delamination event depends on the material properties of the paperboard as well. Delamination of paperboard is often observed to occur fairly close to the printing surface as shown in Fig. 1, resulting in a wavelike appearance of the printed surface (cf. Fig. 2). This may even occur in multiply paperboard where the weakest interface is located near the reverse printing side of the paperboard.

Several test methods, e.g. Z-strength (SCAN P 80:98, 1996), Z-toughness (Lundh and Fellers, 2001) and Scott Bond test (Tappi T 403, 2000), have been developed for measuring the delamination strength of paperboard. From these tests alone it is difficult to judge whether delamination in a specific printing operation will occur or not. In fact, these test methods may not even place different paperboards in their correct order of precedence regarding their ability to resist delamination during printing (cf. Lundh, 2003). The reason is that none of these tests are carried out under loading conditions that are representative of the loading situation prevailing at the exit of a printing nip. For instance, while the Z-strength test measures the stress required to separate the weakest interface of the paperboard, stress gradients due to the current loading situation may cause the paperboard to separate at another (stronger) interface in the paperboard.

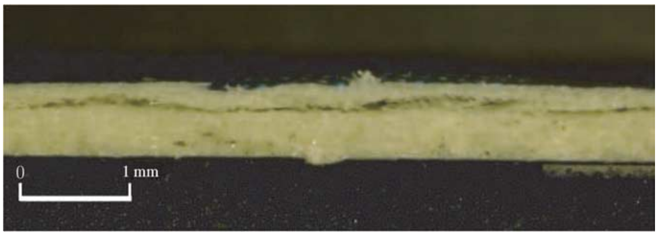

Fig. 1. Cross-section of ink-tack induced delamination in paperboard.

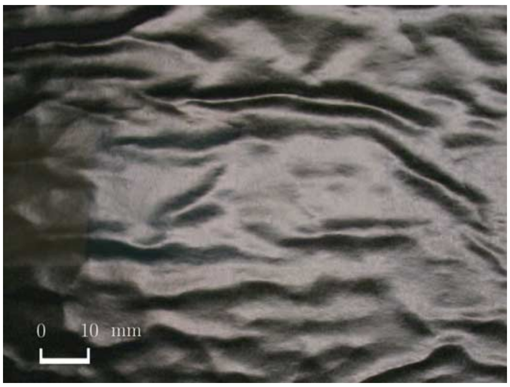

Fig. 2. A surface of a delaminated paperboard with wavelike appearance on the printed surface.

Hence the delamination event depends on a combination of the through-thickness Z-strength variation and the out-of-plane stresses acting in the paperboard, as a result of the loading applied to the board. Considering the number of parameters involved, it is realized that it is far from trivial to assess these dependencies, and theoretical tools are developed to assist in such analysis.

The aim of the present study is to numerically analyze the propensity for ink-tack delamination in paperboard with respect to different through-thickness strength and paperboard ply stiffness distributions.

2. Materials and methods

2.1. Geometry and boundary conditions

The geometrical description of the problem is depicted in Fig. 3. The paperboard passes through a printing nip where the viscosity of the ink causes the paperboard to stick to the printing roll. The distance the paperboard sticks to the printing roll is called the ink-tack length. The ink-tack length, l, is in Fig. 3 given by the radius of the roll, R, multiplied with a segment of the roll defined by the angle, φ, i.e. $l = R\varphi$. The speed of the web is denoted by v and the web tension by σ. The situation is further simplified by assuming that the ink-tack could be modeled as an imposed displacement on the board, and that the paperboard leaves the roll at the angle φ without any remaining forces between the paperboard and the roll. Hence the gradual decrease of the ink-tack force due to ink filamentation is neglected. With this assumption the problem under consideration can be illustrated as shown in Fig. 4. The upper sketch in Fig. 4 shows the ink-tack region, i.e. the region where the paperboard sticks to the roll, in greater detail. The displacement boundary condition in this region is given by

$$\begin{aligned} u_x &= R\left(\sin\frac{x'}{R} - \frac{x'}{R}\right) \\ u_y &= R\left(1 - \cos\frac{x'}{R}\right) \end{aligned} \tag{1}$$

where u_x and u_y denotes the displacement in the x- and y-direction, respectively. The range of the coordinate x' in Eq. (1) is $0 \leqslant x' \leqslant l$.

To accurately model the loading history under steady state conditions for the moving web the displacement field is translated using the transformation

$$x' = x - c(t) \tag{2}$$

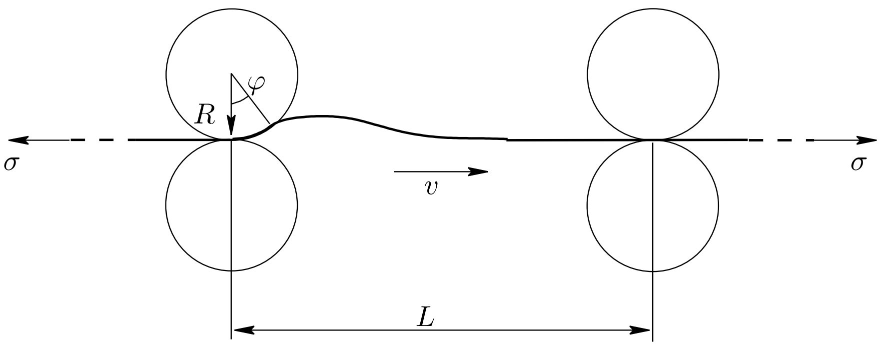

Fig. 3. A sketch of a paperboard passing through printing nips.

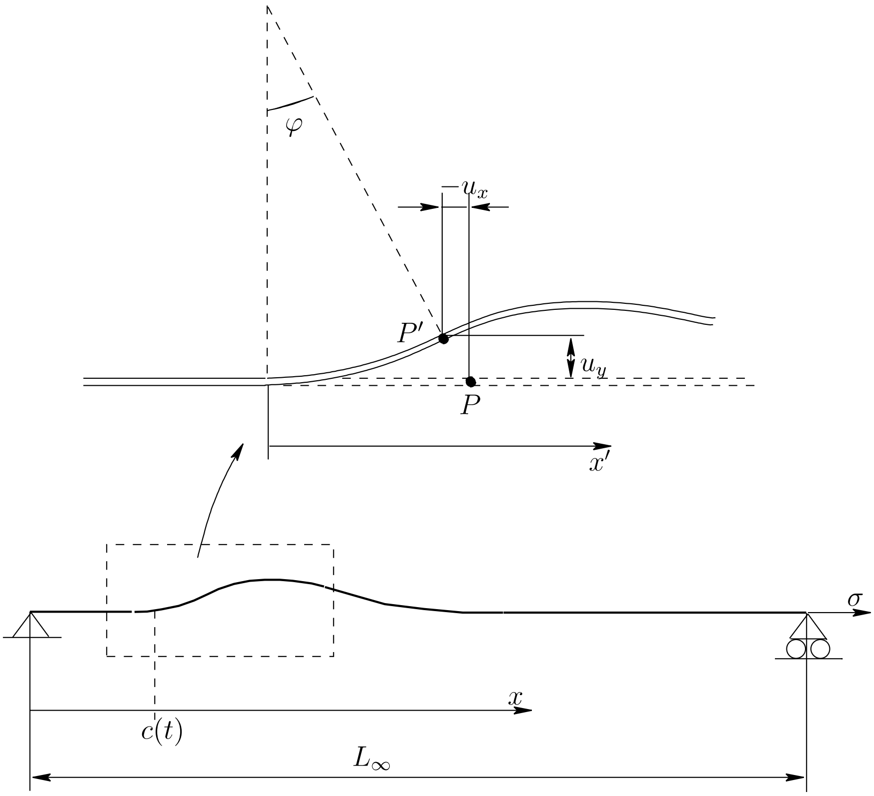

Fig. 4. Boundary conditions acting on a paperboard passing through a printing nip. The upper sketch shows a magnification of the ink-tack region.

where

$$c(t) = x_0 - vt \tag{3}$$

is the x-coordinate of the trailing edge of the ink-tack region. Initially, i.e. at $t = 0$, the trailing edge of the ink-tack region is located at $x = x_0$.

In the analysis we assume that the distance between the printing nips is large enough so that the influence of this distance could be neglected. In practice this is a good approximation since the distance between the printing nips is large enough in comparison to other characteristic dimensions of the problem, such as the thickness of the paperboard, the roll radius and the ink-tack length. For example by comparing the case in which the distance between the printing nips, L, is truly infinite, i.e. $L \to \infty$, by the case when the distance between the printing nips is $L = 140$ mm (when $x_0 = 40$ mm) gives less than 6% difference in bending moment at the exit of the printing nip (for a realistic value of the flexural rigidity of the paperboard). This discrepancy was considered as negligible for the present purposes. The web tension, printing roll radius and ink-tack length were assigned values typical for offset printing operations of paperboard. The values are given in Table 1. Note that considerable uncertainties prevail regarding realistic values of l.

2.2. Material behavior

Paper and paperboard are known to be highly anisotropic materials. The anisotropy originates from the alignment of fibres during the manufacturing of the paper product. The elastic modulus in the machine

Table 1
Model parameters

Parameter	Value
R (mm)	150
l (mm)	20
σ (MPa)	3.75

direction, MD, is typically 2–4 times higher than the elastic modulus in the cross-machine direction, CD, while the through-thickness direction, ZD, has an elastic modulus that is one or two order of magnitudes lower. The MD, CD and ZD are the principle material axes of the material, which means that paper and paperboard are orthotropic. We consider a multilayered paperboard consisting of four layers, schematically shown in Fig. 5. The thickness of the layers is assumed to be constant and equal to 0.1 mm (i.e. $t_A = t_B = t_C = t_D = 0.1$ mm), giving a total paperboard thickness of 0.4 mm. The paper layers are modeled with a linear orthotropic elastic continuum mechanical model, while the bonding between the layers are modeled using an orthotropic elastic–plastic cohesive interface model. This method of modeling paperboard has previously been used by Xia (2002), based on observations of paperboard deformation and fracture in the ZD carried out in Stenberg et al. (2001), Dunn (2000) and Smith (1999).

2.2.1. Interface behavior

The interface behavior is described by an orthotropic elastic–plastic cohesive law which relates the interface traction to the opening and sliding of the interface (cf. Xia, 2002). The opening and sliding of the interface is divided into an elastic and a plastic cohesive part according to

$$\delta_i = \delta_i^e + \delta_i^p \tag{4}$$

where the subindex $i = 1$, $i = 2$ and $i = 3$ refers to the MD, CD and ZD, respectively (cf. Fig. 6). Hence, the subindex $i = 1$ and 2 in Eq. (4) refers to the sliding of the interface and the subindex $i = 3$ refer to the opening of the interface. Note that Eq. (4) refers to the local coordinate system in the interface as shown in Fig. 6. The change in the traction vector, T_i, across the interface due to incremental relative displacements is governed by

$$\Delta T_\alpha = K_\alpha(\bar{\delta}^p)(\Delta\delta_\alpha - \Delta\delta_\alpha^p) \tag{5}$$

where $K_\alpha(\bar{\delta}^p)$ denotes the components of the instantaneous interface stiffness in the α-direction and $\bar{\delta}^p$ denotes the equivalent plastic displacement. Note that greek letters implies that no summation should be carried out over repeated indices. Since we consider a two-dimensional case in the MD–ZD plane, α is either 1

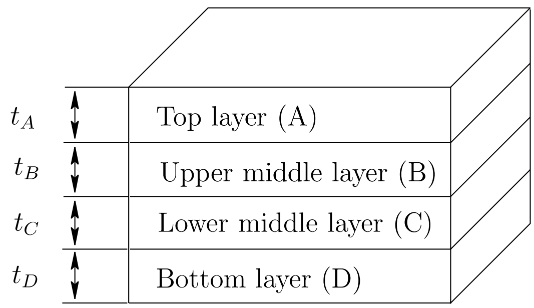

Fig. 5. A paperboard consisted of four layers.

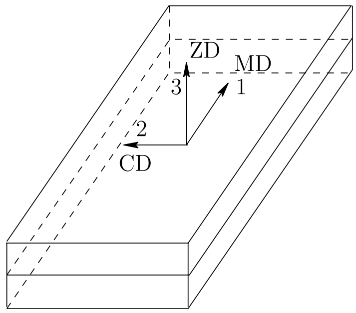

Fig. 6. Coordinate system in the interface.

or 3. In the continuation of this outline we restrict ourselves to this particular case. The instantaneous interface stiffness depends on the equivalent plastic displacement, $\bar{\delta}^{\mathrm{p}}$, according to

$$K_\alpha(\bar{\delta}^{\mathrm{p}}) = K_\alpha^0[1 - R_\alpha^k D(\bar{\delta}^{\mathrm{p}})] \tag{6}$$

where $D(\bar{\delta}^{\mathrm{p}})$ is the interface damage derived as

$$D(\bar{\delta}^{\mathrm{p}}) = \tanh(C\bar{\delta}^{\mathrm{p}}) \tag{7}$$

and K_α^0 is the initial interface stiffness. The R_α^k and D in Eq. (6), and C in Eq. (7), are material constants.

Yielding occurs in the interface when

$$f(T, \bar{\delta}^{\mathrm{p}}) = \frac{S_3(\bar{\delta}^{\mathrm{p}})}{S_1(\bar{\delta}^{\mathrm{p}})^2} T_1^2 + T_3 - S_3(\bar{\delta}^{\mathrm{p}}) = 0 \tag{8}$$

where f is the yield function and $S_\alpha(\bar{\delta}^{\mathrm{p}})$ are the instantaneous interface strengths which depends on the equivalent plastic displacement, $\bar{\delta}^{\mathrm{p}}$, according to

$$S_\alpha(\bar{\delta}^{\mathrm{p}}) = S_\alpha^0[1 - R_\alpha^{\mathrm{s}} D(\bar{\delta}^{\mathrm{p}})] \tag{9}$$

where S_α^0 are the initial interface strengths and R_α^{s} are material constants. The evolution of the interface stiffness and strength are shown schematically in Fig. 7. The plastic flow rule may be written as

$$\Delta\delta_\alpha^{\mathrm{p}} = \chi M_\alpha \Delta\bar{\delta}^{\mathrm{p}} \tag{10}$$

where M_α are the components of the unit flow direction, i.e.

$$M_\alpha = \frac{\hat{M}_\alpha}{\sqrt{\hat{M}_k \hat{M}_k}} \tag{11}$$

and χ behaves such that

$$\chi = \begin{cases} 1 & \text{if } f = 0 \text{ and } T_\alpha \Delta\delta_\alpha^{\mathrm{p}} > 0 \\ 0 & \text{if } f < 0 \text{ or } f = 0 \text{ and } T_\alpha \Delta\delta_\alpha^{\mathrm{p}} < 0 \end{cases} \tag{12}$$

For non-associated flow the components of the plastic flow direction may be expressed as

$$\begin{aligned} \hat{M}_1 &= \frac{\partial f}{\partial T_1} = 2\frac{S_3(\bar{\delta}^{\mathrm{p}})}{S_1(\bar{\delta}^{\mathrm{p}})^2} T_1 \\ \hat{M}_3 &= \mu(\bar{\delta}^{\mathrm{p}}) \frac{\partial f}{\partial T_3} = \mu(\bar{\delta}^{\mathrm{p}}) \end{aligned} \tag{13}$$

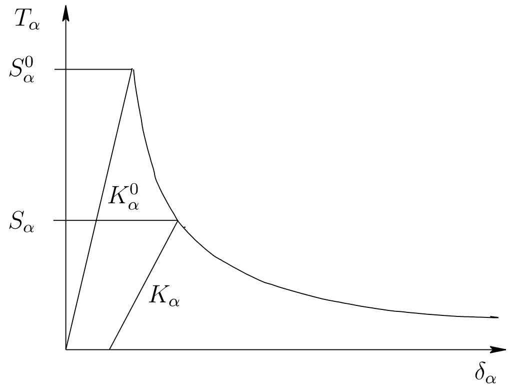

Fig. 7. Interface behavior.

where μ is a frictional function which depends on the equivalent plastic displacement (note that $\mu = 1$ corresponds to associated flow). In this case

$$\mu = A[1 - BD(\bar{\delta}^{\mathrm{p}})] \tag{14}$$

where A and B are material constants.

The interface model defined by Eqs. (4)–(14) was implemented in an UINTER subroutine to be used in conjunction with the general purpose finite element code ABAQUS/Standard (ABAQUS Inc., 2003). Within this framework, penetration of the paper layers is prevented by using a penalty stiffness in compression which increases exponentially with the penetration depth. The interface model was used to model the interaction between the top layer and the upper middle layer, and between the middle layers of the board. The bottom layer was assumed to be perfectly bonded to the lower middle layer. This assumption was made primarily due to computational efficiency reasons. Thus we consider delamination between the uppermost and the middle layers of the board.

The material constants used in the analysis were estimated by aid of Xia (2002) based on measurements using the modified Arcan device (Stenberg et al., 2001). All parameters but the initial yield stresses (cf. Fig. 7), were taken to be same in both interfaces, and are reported in Table 2.

2.2.2. Continuum behavior

Each paper layer was assumed to be linear orthotropic elastic. The in-plane moduli and poisson ratio used in this analysis were chosen as values that are commonly found in paperboard which is used

Table 2
Interface constants

Parameter	Value
K_1^0 (MPa/mm)	800
K_3^0 (MPa/mm)	400
R_1^k	0.875
R_3^k	0.97
R_1^s	0.875
R_3^s	0.97
A	0.28
B	0.99
C	11.0

for packages. Based on the elastic modulus in MD, E_1, the elastic modulus in CD, E_2, and the in-plane shear modulus, G_{12}, were chosen as

$$\begin{aligned} E_2 &= \frac{1}{3}E_1 \\ G_{12} &= \frac{2}{9}E_1 \end{aligned} \tag{15}$$

The in-plane poisson ratio was chosen as

$$v_{12} = 0.3 \tag{16}$$

Note that the linear elastic properties are referring to the same coordinate system as is used for the interface properties shown in Fig. 6.

Data for the out-of-plane moduli and poisson ratio can be found in Xia (2002), Baum (1987) and Persson (1991). Here we set the out-of-plane modulus to one-hundredth of the elastic modulus in MD, while the transverse poisson ratios were assumed to be zero, i.e.

$$\begin{aligned} E_3 = G_{13} = G_{23} &= \frac{1}{100}E_1 \\ v_{13} = v_{23} &= 0 \end{aligned} \tag{17}$$

In many cases the outermost layers of multilayered paperboard are made of chemical pulp, whereas the middle layers are made of mechanical pulp. The chemical pulp layers have a higher tensile stiffness than the mechanical pulp layers. Measurements on the individual layers of a multilayered paperboard indicates that the tensile stiffness of the chemical and mechanical pulp layers could differ by up to a factor of three (see Xia, 2002). Commercially there are paperboard where all the plies are made of the same kind of pulp, so that the material properties are virtually identical throughout the board. As a measure of the difference in elastic modulus between the outermost and the middle layers we introduce a stiffness ratio, r_{E}, defined as

$$r_{\mathrm{E}} = E_1^{BC}/E_1^{AD} \tag{18}$$

where E_1^{AD} is the elastic modulus in the MD for the top and bottom layer and E_1^{BC} is the elastic modulus in the MD for the middle layers (cf. Fig. 5). In this work we consider paperboard with the stiffness ratio, r_{E}, equal to 1/3, 2/3 and 1. Assuming furthermore that the flexural rigidity is constant, the elastic moduli in MD are given in Table 3. The behavior of an individual layer is completely defined by the elastic modulus in the MD and Eqs. (15)–(17).

2.3. FE-modeling

The analysis were carried out using the general purpose finite element code ABAQUS/Standard. The analysis were divided into five steps: In the first step the web-tension was applied. In the second step the initial ink-tack was applied. The moving boundary condition according to Eqs. (1)–(3) was applied in the third step. In the fourth step the web was released from the roll and in the last step, the web tension

Table 3
MD elastic moduli for the paper layers

r_{E}	E_1^{AD} (MPa)	E_1^{BC} (MPa)
1/3	9000	3000
2/3	8609	5739
1	8250	8250

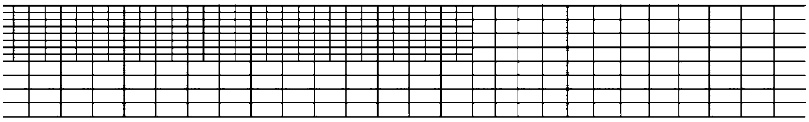

Fig. 8. A close-up of the FE-mesh at $x = 40$.

was removed. Note that a condensed mesh was used to model the part of web that is adhered to the roll. A close up of the mesh used in the analysis is shown in Fig. 8. The mesh comprised a total of 10316 nodes and 7800 bi-linear elements. Plane strain conditions were assumed.

After completion of the analysis, the average plastic displacement (i.e. remaining displacement) in the interface was used as a measure of the interface delamination. The average plastic displacement was computed as

$$\hat{\delta}_{\alpha}^{\mathrm{p}} = \frac{1}{(x_2 - x_1)} \int_{x_1}^{x_2} \delta_{\alpha}^{\mathrm{p}} \, \mathrm{d}x \tag{19}$$

where $\alpha = 1, 3$ and x_1 and x_2 are points along the web. $\delta_{\alpha}^{\mathrm{p}}$ is expected to be constant since a uniform interface behavior is assumed. The result, however, indicated a slight variation, probably due to numerical disturbances in the solution and the finite value of the length between the printing nips which was used in the analysis. To numerically determine Eq. (19), the length between the points $(x_2 - x_1)$ was chosen to be ten times the thickness of the board, i.e. $(x_2 - x_1) = 4$ mm. The variation of $\delta_{\alpha}^{\mathrm{p}}$ within this domain was below 10%.

In order to study the effect of different interface strengths, a parameter r_{S}, called the interface strength ratio, is defined as

$$r_{\mathrm{S}} = \frac{S_3^{0B-C}}{S_3^{0A-B}} = \frac{S_1^{0B-C}}{S_1^{0A-B}} \tag{20}$$

Analysis were carried out with values of r_{S} equal to 1, 0.8, 0.6 and 0.4. These situations were accomplished by varying the initial yield stresses of the *B–C* interface, while keeping the initial yield stresses of the *A–B* interface, i.e. S_1^{0A-B} and S_3^{0A-B}, constant at 1.2 MPa and 0.4 MPa, respectively.

In total 12 different input combinations of the stiffness ratio, r_{E}, and interface strength ratio, r_{S}, were used in the analysis in order to investigate the ink-tack phenomena.

3. Results

Fig. 9 shows the σ_{11}-stress distribution during continuing ink-tack delamination for three different combinations of r_{E} and r_{S}.

The case where $r_{\mathrm{E}} = r_{\mathrm{S}} = 1$, corresponding to a paperboard with the same board properties in all the layers and the same interface strength in the interface between the layers, is shown in Fig. 9(a). From the σ_{11}-stress distribution in Fig. 9(a), it can be observed that a region of high tension stress extends from the point where the paperboard is released from the roll. The tension stress exceeds 40 MPa at the surface of the uppermost layer over a distance approximately equal to the thickness of the board. This stress level is normally sufficient to cause permanent deformation in paperboard made of chemical pulp. The highest compression value in the bottom layer is approximately −30 MPa. The corresponding delamination pattern after unloading of the web is shown in Fig. 10(a). Note that the paperboard remains fairly straight in the case where the board delaminates predominantly between the top ply and the upper middle layer.

The cases when $r_{\mathrm{E}} = 0.67$, $r_{\mathrm{S}} = 0.6$ and $r_{\mathrm{E}} = 0.33$, $r_{\mathrm{S}} = 0.4$, Fig. 9(b) and (c), respectively, corresponds to multilayered paperboards where the outermost layers have a higher elastic modulus than the middle layers, and the interface strength in the interface between the top and upper middle layer is higher than the

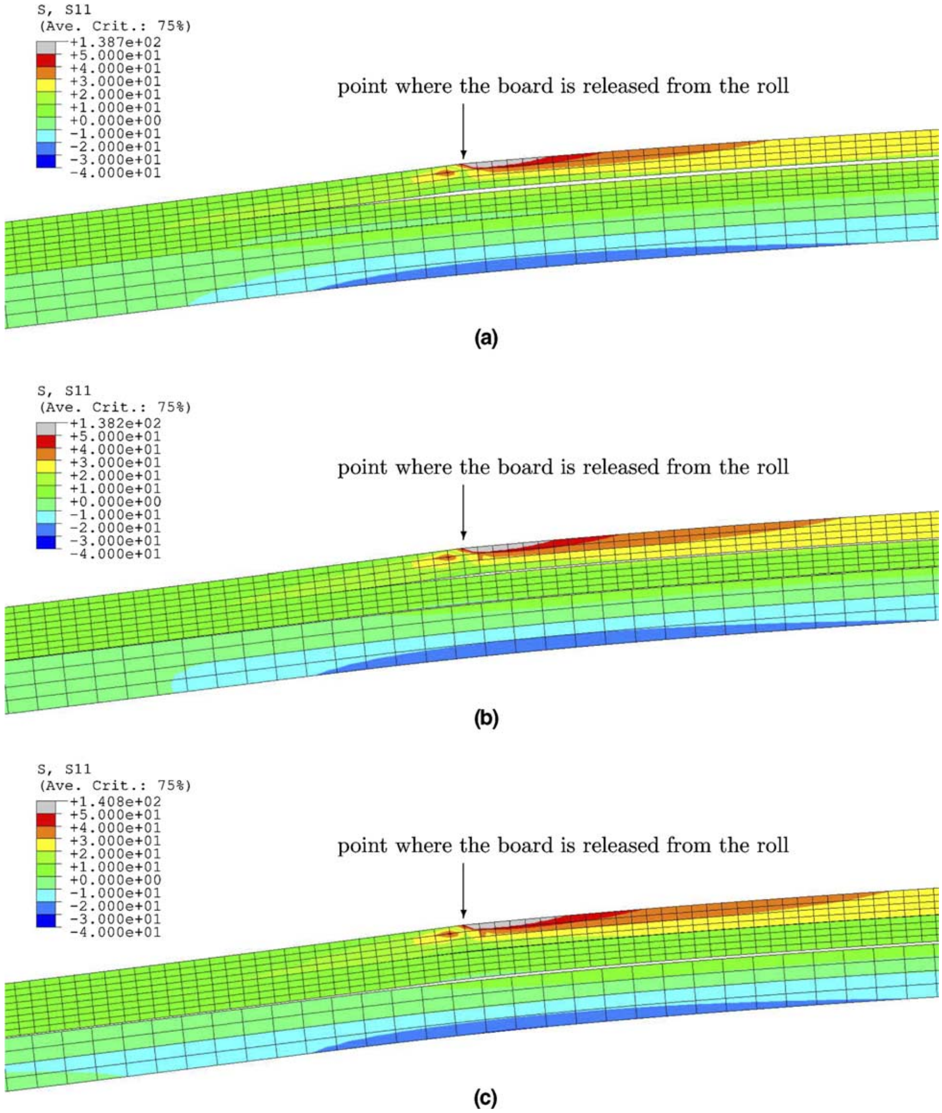

Fig. 9. The σ_{11}-stress distribution at stage 3 for (a) $r_S = r_E = 1$, (b) $r_E = 0.67$, $r_S = 0.6$ and (c) $r_E = 0.33$, $r_S = 0.4$.

strength of the interface between the middle layers. From the σ_{11}-stress distribution in Fig. 9(b) and (c), it can be observed that high tension stresses prevail in a region similar to the tension zone in Fig. 9(a). The corresponding delamination patterns after unloading of the web are shown in Fig. 10(b) and (c), respectively. By comparing the delamination pattern in Fig. 10(a)–(c), it is observed that as the interface strength between the middle layers decreases, delamination will be more prominent in the interface between the middle layers, ultimately resulting in a single delamination between the middle layers. It is further noted that the unloading of the web results in permanent deflection of the board for the cases when $r_E = 0.67$, $r_S = 0.6$ and $r_E = 0.33$, $r_S = 0.4$ (cf. Fig. 10(b) and (c)), respectively. This is a consequence of the fact that delamination between the middle layers is mainly governed by shear, as opposed to the delamination between the outer layers, which is dominated by opening. This fact is revealed by Figs. 11 and 12.

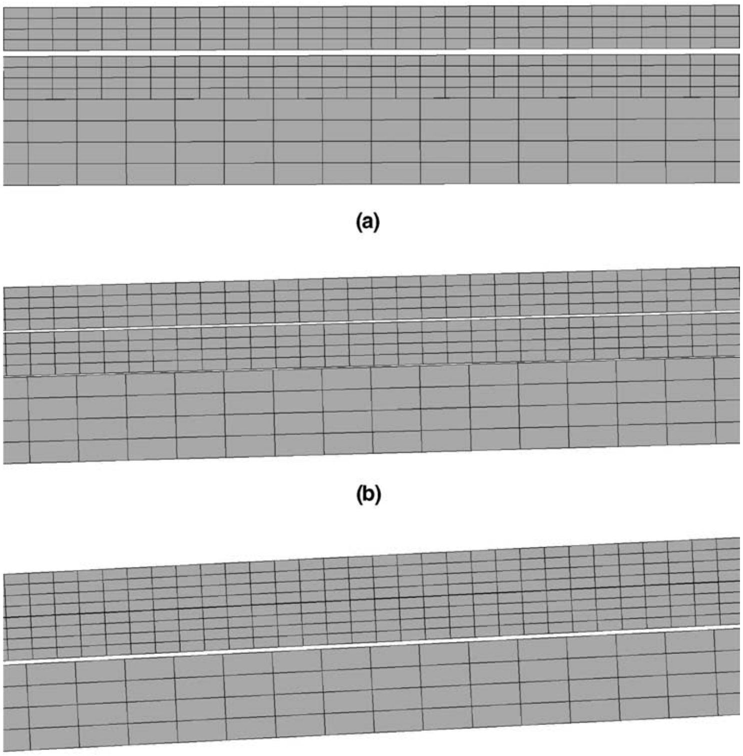

(a)

(b)

(c)

Fig. 10. Delamination pattern after unloading, i.e. stage 5, for (a) $r_E = r_S = 1$, (b) $r_E = 0.67$, $r_S = 0.6$ and (c) $r_E = 0.33$, $r_S = 0.4$.

In Fig. 11 is the ratio of the average plastic sliding displacement to the average plastic opening displacement, $\hat{\delta}_1^p/\hat{\delta}_3^p$, plotted as function of the interface strength ratio, r_S, for the stiffness ratios, $r_E = 1$, $r_E = 0.67$ and $r_E = 0.33$. For interface *B–C*, i.e. the interface between the middle layers, it is seen in Fig. 11 that the sliding mode dominates the delamination for nearly all combinations of the stiffness ratio and the interface strength ratio.

For interface *A–B*, i.e. the interface between the top and the upper middle layer, it is seen that the ratio of the average plastic sliding displacement to the average plastic opening displacement, $\hat{\delta}_1^p/\hat{\delta}_3^p$, increases approximately from 0.1 to 0.25 as the the interface strength ratio, r_S, increases from 0.4 to 1. Thus the opening mode dominates the delamination in interface *A–B*, for all the investigated combinations of the stiffness ratio and the interface strength ratio.

In Fig. 12 is the average plastic opening displacement, $\hat{\delta}_3^p$, as function of the interface strength ratio, r_S, for the different values of the stiffness ratio, r_E, shown. In Fig. 12, it is apparent that the delamination opening dominates in the interface *A–B* for $r_S > 0.6$, which probably is the case for most commercial paperboard grades cf. Xia (2002). The shift from delamination in the outermost interface *A–B* to the inner interface *B–C* does not depend significantly on the stiffness ratio r_E.

For $r_S < 0.5$, the delamination opening, $\hat{\delta}_3^p$, is several times greater in interface *B–C* than in interface *A–B* (cf. Fig. 12). For the cases when $r_E = 0.67$, $r_S = 0.6$ and $r_E = 0.33$, $r_S = 0.4$ the average plastic sliding displacement, $\hat{\delta}_1^p$, is approximately 2.5 and 1.5 times greater than the average plastic opening displacement, $\hat{\delta}_3^p$, respectively (cf. Fig. 11). This gives that the delamination between the middle layers is mainly governed by shear for the cases in Fig. 10(b) and (c).

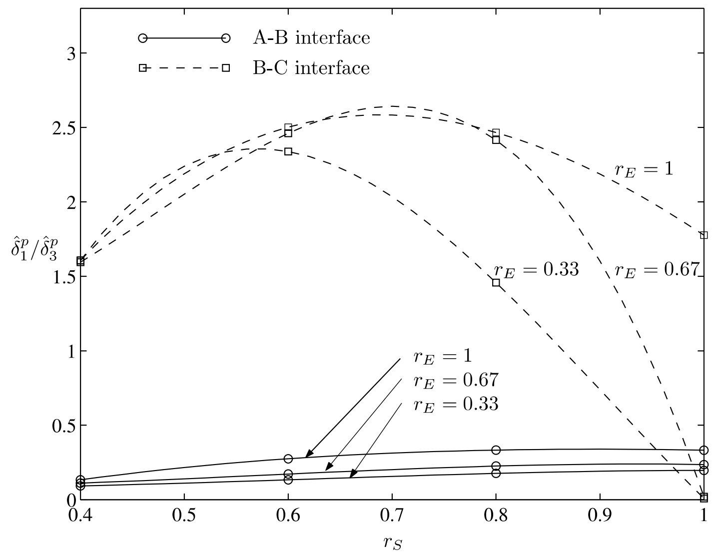

Fig. 11. The ratio of average plastic opening displacement to average plastic sliding displacement as a function of the interface strength ratio, r_S, for the stiffness ratios, $r_E = 1$, $r_E = 0.67$ and $r_E = 0.33$.

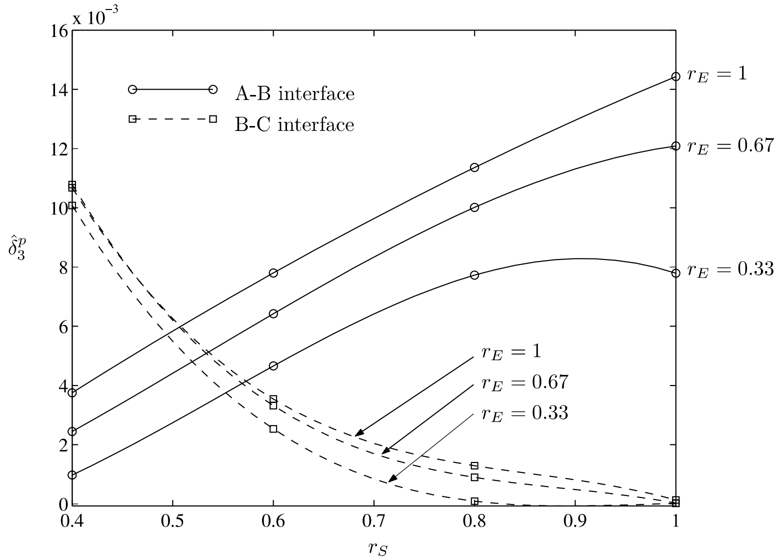

Fig. 12. Average plastic opening displacement as a function of the interface strength ratio, r_S, for the stiffness ratios, $r_E = 1$, $r_E = 0.67$ and $r_E = 0.33$.

The cohesive zone in front of the separation point at the interfaces between the plies at step 3 in the analysis depends on the stiffness ratio, r_E, and the interface strength ratio, r_S. For the case when $r_E = r_S = 1$ the opening mode dominates over the sliding mode and the simulation gives a cohesive zone in front of the separation point that has a length that is of the same order of magnitude as the thickness of the paperboard. However, for the case when $r_E = 0.33$ and $r_S = 0.4$, i.e. when the delamination occurs due to shear between the middle plies, the cohesive zone in front of the separation point has a length that is up to ten times the length of the thickness of the paperboard.

4. Discussion and conclusions

The maximum σ_{11}-stress levels in tension in Fig. 9 are normally sufficient to cause permanent deformation in paperboard made of chemical pulp. Hence the uppermost layer would remain longer than the other layers after unloading of the board. The wave-like appearance of the printed board seen in Fig. 2 may be due to a combination of this fact in conjunction with the fact that the interface strength is not constant but varies as function of the location in the board. The fact that the out-of-plane strength of paperboard is essentially insensitive to the presence of pre-existing cracks or delamination, as shown in Girlanda et al. (2005), is also important in this respect. Neither plasticity nor variations in the interface strengths are taken into account in the present study. In the vicinity of the point where the web is released from the roll, the stresses becomes infinite. This behavior is an effect of the displacement boundary condition applied to the board, which yields a worst case situation. In reality, the release of the web from the roll is a more gradual process involving ink-filamentation and rupture. The stress singularity observed in the present analysis would thus be somewhat relaxed.

From Fig. 12, it is evident that any out-of-plane test in which the weakest interface in the board is tested (e.g. the Z-strength test, the Z-toughness test, the Scott bond test) would be of less value to predict inc-tack delamination, in most cases. From Fig. 11 it is also clear that a primary measure to improve the printability of paperboard would be to improve the opening resistance against delamination in the uppermost interface.

To summarize, the following conclusions could be drawn from the present study:

- Delamination occurs in the outermost interface, although the interface strength may be lower further below in the board. The delamination opening dominates in the outermost interface for interface strength ratios $r_S > 0.6$, for realistic values of the elastic stiffness ratio between the outer- and inner-most paper plies. This observation helps to explain why simple tests for the out-of-plane strength of paperboard like the Z-strength test are inconclusive when it comes to predict ink-tack delamination during offset printing.
- The delamination opening in the outermost interface decreases as the stiffness ratio decreases. The delamination opening in the inner interface seems, on the other hand, to be essentially unaffected by the magnitude of this ratio.
- The delamination in the inner interface is predominantly governed by shear, while the delamination in the outermost interface is predominantly governed by opening, at least for the relation between the interface strengths used in the present analysis.

Future efforts within this area may involve the incorporation of plasticity models to model the continuum behavior of the paper plies. Such models have been presented in Mäkelä and Östlund (2003) and Xia et al. (2002), although in this case a simpler one-dimensional model would suffice. Along with a varying interface strength this may result in more realistic delamination patterns and perhaps also more accurate quantitative predictions of ink-tack delamination. Another item not being addressed in the present work is the effect of the coating. It is believed that the coating mainly influences the printability by influencing the ink-tack force. Although delamination between the coating and the paperboard substrate is seldom observed, it is believed that this could be modeled in a similar manner as the delamination between the paper plies, provided that a reasonably accurate model for the interaction between the coating and the paper substrate exists.

Another item than could be more thoroughly explored is the influence of the displacement boundary condition to simulate ink-tack. The constitutive behavior of the ink could be implemented into an interface model to model the interaction between the printing roll and the paperboard in a more realistic manner. Again, of course, a realistic model for the behavior of the ink is needed.

Although the analysis presented in this report aims to investigate the performance of paperboard subjected to ink-tack in offset printing, it should be mentioned that the results also apply to PE-lamination of paperboard. In that case the cohesive force between the roll and the board is due to the adhesion between the roll and the PE-layer attached to the board in the form of a thin film dissolution.

Acknowledgements

The authors wish to thank Prof. Christer Fellers and Prof. Sören Östlund for their valuable advice. STFI partner companies participating in the research cluster 'The Engineered Board' are gratefully acknowledged.

References

ABAQUS Analysis User's Manual, Version 6.4. 2003. ABAQUS, Inc., Pawtucket, RI.

Baum, G.A., 1987. Elastic properties of paper. In: Kolseth, P., Fellers, C., Salmén, L., Rigdahl, M. (Eds.), Design Criteria for Paper Performance. STFI, Stockholm, pp. 1–27.

De Grâce, J.H., Dalphond, J.E., Mangin, P.J., 1992. A mechanistic approach to ink transfer. Part III: Properties of Ink Filaments in Printing Nips. Advances in Printing Science and Technology 21, 312–327.

Dunn, H., 2000. Micromechanisms of paperboard deformation, MS Thesis. Department of Mechanical Engineering, Massachussetts Institute of Technology, Cambridge, MA.

Ercan, S.N., Bousfield, D.W., 2000. Influence of fluid rheology on filament size. In: 2000 TAPPI International Printing and Graphic Arts Conference Proceedings.

Franklin, A.T., 1980. Paper/ink/press relationships. Professional Printer 24 (2), 2–5.

Girlanda, O., Hallbäck, N., Östlund, S., Tryding, J., 2005. Defect sensitivity and strength of paperboard in the out-of-plane tension and shear. Journal of Pulp and Paper Science 31 (2), 100–104.

Lundh, A., Fellers, C., 2001. The Z-toughness method for measuring delamination resistance of paper. Nordic Pulp and Paper Research Journal 16 (4), 298–305.

Lundh, A., 2003. Characterisation of delamination properties in paper materials, Licentiate Thesis. Department of Fibre and Polymer Technology, Royal Institute of Technology, Stockholm, Sweden.

Mäkelä, P., Östlund, S., 2003. Orthotropic elastic–plastic material model for paper materials. International Journal of Solids and Structures 40, 5599–5620.

Persson, K., 1991. Material model for paper, experimental and theoretical aspects. Department of Solid Mechanics, Lund Institute of Technology, Lund, Sweden.

SCAN P 80:98, 1996. Z-directional tensile strength.

Smith, C.A., 1999. Micromechanics of the through-thickness deformation of paperboard, MS Thesis. Department of Mechanical Engineering, Massachussetts Institute of Technology, Cambridge, MA.

Stenberg, N., Fellers, C., Östlund, S., 2001. Measuring the stress–strain of paperboard in the thickness direction. Journal of Pulp and Paper Science 27, 213–221.

TAPPI T 403, 1985. Bursting strength of paper.

Xia, Q.S., 2002. Mechanics of inelastic deformation and delamination in paperboard, PhD Thesis. Department of Mechanical Engineering, Massachussetts Institute of Technology, Cambridge, MA.

Xia, Q.S., Boyce, M.C., Parks, D.M., 2002. A constitutive model for the anisotropic elastic–plastic deformation of paper and paperboard. International Journal of Solids and Structures 39, 4053–4071.